MATERIALS CHEMISTRY FRONTIERS

RESEARCH ARTICLE

View Article Online
View Journal | View Issue

Cite this: *Mater. Chem. Front.*, 2025, **9**, 3583

Precision imaging of superoxide anion radicals *in vivo* using a bicyclic dioxetane chemiluminescent nanoprobe

Silin Huang,†[c] Min Shi,†[b] Jia-Xing Chen,†[a] Peng-Fei Shi *[b] and Xue-Qiang Wang *[ac]

Received 19th August 2025,
Accepted 4th November 2025

DOI: 10.1039/d5qm00620a

rsc.li/frontiers-materials

Accurate detection of disease-related reactive oxygen species (ROS), such as superoxide anion radicals ($O_2^{\bullet-}$), is essential for the diagnosis and treatment of inflammation or cancer. Herein, we report the development of a novel chemiluminescent nanoprobe, C10-SPN, based on chemiluminescence resonance energy transfer (CRET) for highly sensitive and specific detection of $O_2^{\bullet-}$ *in vitro* and *in vivo*. The obtained nanoprobe exhibited efficient energy transfer, a red-shifted emission peak at 680 nm, and an extended chemiluminescence half-life of up to 7 min. C10-SPN demonstrated excellent selectivity toward $O_2^{\bullet-}$ over other biologically relevant species, low cytotoxicity, and strong biocompatibility. *In vivo* imaging in mouse models of peritonitis and breast cancer confirmed the capability of C10-SPN to visualize $O_2^{\bullet-}$ levels with high contrast, enabling discrimination between normal and diseased tissues. This study highlights C10-SPN as a promising tool for $O_2^{\bullet-}$-responsive imaging and early disease diagnosis.

Reactive oxygen species (ROS) play a critical role in various physiological and pathological processes, including cellular signaling, immune response, and disease progression.[1] Among ROS, the superoxide anion radical ($O_2^{\bullet-}$) is one of the most significant, acting as a primary ROS that can further generate other reactive species such as hydrogen peroxide (H_2O_2) and hydroxyl radicals ($^{\bullet}OH$).[2] The precise detection and imaging of $O_2^{\bullet-}$ *in vivo* are crucial for understanding its biological functions and its involvement in diseases such as cancer, neurodegenerative disorders, and inflammatory conditions.[3] However, achieving accurate and real-time imaging of $O_2^{\bullet-}$ in living systems remains a significant challenge due to its short lifespan, low concentration, and high reactivity.[4]

Traditional methods for detecting $O_2^{\bullet-}$, such as electron paramagnetic resonance (EPR) spectroscopy and fluorescence-based probes, often suffer from limitations in sensitivity, specificity, and spatial–temporal resolution.[5] Moreover, many existing probes are unsuitable for *in vivo* applications due to issues such as limited penetration depth and interference from other ROS. Therefore, there is an urgent need for advanced nanoprobes that can overcome these limitations and enable precise imaging of $O_2^{\bullet-}$ in complex biological environments.[6]

In recent years, chemiluminescent (CL) probes have emerged as a promising tool for ROS detection due to their high sensitivity, low background noise, and ability to operate without external light excitation.[7] Among these, dioxetane-based chemiluminescent probes have garnered significant attention because of their unique mechanism of light emission upon reaction with specific ROS.[8] The conventional chemiluminescence imaging methods for detecting $O_2^{\bullet-}$ still face significant application challenges due to drawbacks such as low emission intensity, short emission wavelength, and brief chemiluminescence duration.[9] Chemiluminescence based on resonance energy transfer (CRET) offers an opportunity to overcome these issues. CRET can effectively extend the luminescence duration and induce a redshift in the emission wavelength.[10] It is, therefore, imperative to develop a chemiluminescence system based on the CRET principle with high sensitivity and strong specificity for the *in vitro* and *in vivo* detection of $O_2^{\bullet-}$. In this study, we developed a novel chemiluminescence system based on CRET by modifying CL probes using a nanoprecipitation method. This system was applied for the *in vitro* and *in vivo* imaging and detection of $O_2^{\bullet-}$ due to its high sensitivity and specificity.

The research commenced with the synthesis of a bicyclic dioxetane chemiluminescent probe featuring an $O_2^{\bullet-}$-responsive aryl triflate group (Fig. 1a). The high nucleophilicity of $O_2^{\bullet-}$ enables it to attack the electron-deficient aryl triflate moiety, inducing a nucleophilic aromatic substitution that cleaves the

[a] *Department of Nuclear Medicine, Zhejiang Cancer Hospital, Hangzhou Institute of Medicine (HIM), Chinese Academy of Sciences, Hangzhou, Zhejiang 310022, China. E-mail: wangxq@hnu.edu.cn*
[b] *School of Chemistry and Chemical Engineering, Linyi University, Linyi 276000, Shandong, P. R. China. E-mail: shipengfei913@163.com*
[c] *Department of Gastroenterology, South China Hospital, Medical School, Shenzhen University, Shenzhen, 518116, China*
† These authors contributed equally.

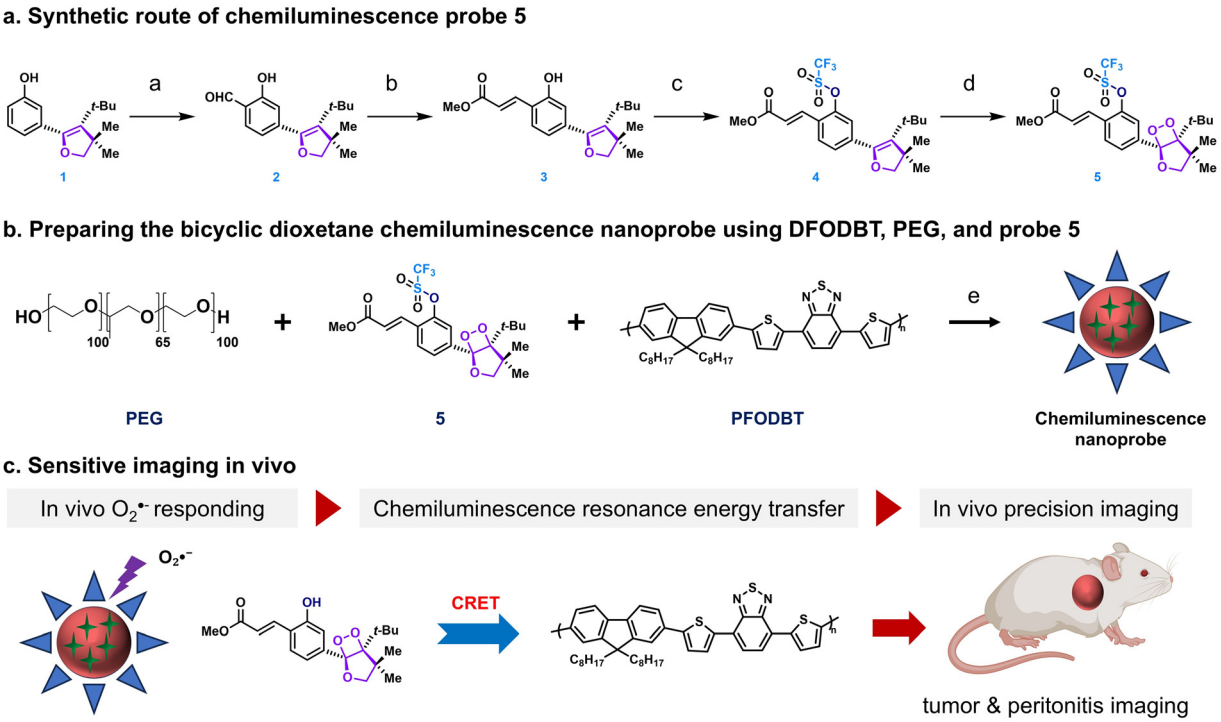

Fig. 1 Design of the C10-SPN probe. (a) Synthetic route of chemiluminescent probe 5; conditions: a. $MgCl_2$, NEt_3, $(CH_2O)_n$, THF, reflux; b. Ph_3PCHCO_2Me, DCM, rt; c. trifluoromethanesulfonic anhydride, Et_3N, DCM, 0 °C–rt; d. TPP, O_2, yellow light, DCM, 0 °C; e. THF/H_2O. (b) Preparing the bicyclic dioxetane chemiluminescent nanoprobe with probe 5. (c) Highly sensitive *in vivo* disease lesion imaging.

triflate group and subsequently activates the chemiluminescent dioxetane scaffold.[11,12] Starting from compound **1**, an efficient *ortho*-carbonylation reaction, mediated by $MgCl_2$, produced compound **2**. Subsequently, a Wittig reaction was employed to convert compound **2** into compound **3**, where the phenolic hydroxyl group was protected by a triflyl group to generate **4**. The final step involved the oxidation of the olefin on the bicyclic ring of **4**, yielding the target dioxetane probe 5. The chemiluminescent nanoprobe (C10-SPN) was then formed *via* nanoprecipitation, combining probe 5 with a PFODBT material in the presence of an amphiphilic triblock copolymer (PEG-*b*-PPG-*b*-PEG) (Fig. 1b). This nanoprobe was designed for precise *in vivo* imaging of disease lesions, leveraging the high sensitivity of the triflyl group to $O_2^{\bullet-}$ and its potential for chemiluminescence resonance energy transfer (Fig. 1c).

We used the amphiphilic substance PEG as a stabilizer to encapsulate probe 5 and PFODBT, rendering the material hydrophilic. To verify that PFODBT, used for resonance energy transfer, was indeed incorporated into the chemiluminescent nanoprobe, we first performed UV characterization of the material. The UV absorption spectrum results showed that the C10-SPN chemiluminescent material exhibited the characteristic absorption peaks of PFODBT at 385 and 550 nm (Fig. 2a), confirming that PEG effectively encapsulated probe 5 and PFODBT, indicating the successful construction of the desired nanoprobe system (Fig. S1).

Fig. 2b demonstrates that the C10-SPN chemiluminescent material emits a strong luminescence signal upon the introduction of $O_2^{\bullet-}$. Owing to the effective incorporation of PFODBT, the chemiluminescence generated by the reaction between $O_2^{\bullet-}$ and the C10 probe efficiently excites PFODBT fluorescence, facilitating energy transfer within the system. This energy relay markedly boosts the overall luminescence intensity and induces a red-shift in the emission peak to 680 nm, thereby enhancing the imaging capability of the nanoprobe.

The morphology and hydrated particle size of the C10-SPN nanoparticles were subsequently characterized in detail. The prepared C10-SPN dispersion was diluted to an appropriate concentration and examined using transmission electron microscopy (TEM). As shown in the inset of Fig. 2c, the nanoparticles displayed a spherical shape with an average diameter of approximately 70 nm. Dynamic light scattering (DLS) analysis further confirmed a hydrated diameter of around 82 nm, indicating good dispersion and colloidal stability in aqueous solution.

To evaluate the selectivity of C10-SPN, a panel of representative cations and reactive species was tested, including Mg^{2+}, Na^+, Cu^{2+}, K^+, Ca^{2+}, Fe^{3+}, Fe^{2+}, H_2O_2, $O_2^{\bullet-}$ and other biologically relevant species (Fig. 2d and Fig. S2). In phosphate-buffered saline (PBS, pH 7.4), the C10-SPN nanoparticles exhibited a pronounced chemiluminescence response selectively to $O_2^{\bullet-}$, while showing minimal or no response to the other analytes tested. These results highlight the high specificity of C10-SPN toward superoxide anions in a complex chemical environment.

To evaluate the relative chemiluminescence intensity of C10-SPN, the material was incubated with $O_2^{\bullet-}$ in a black 96-well plate.

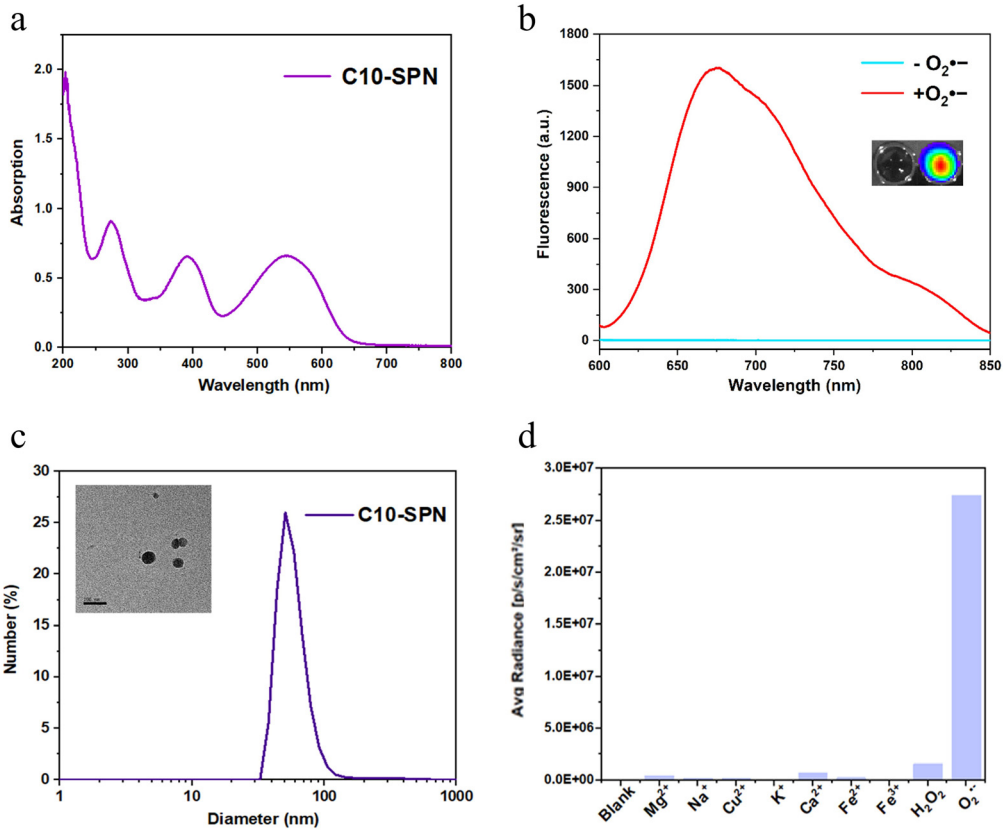

Fig. 2 Basic properties of C10-SPN. (a) The ultraviolet absorption spectrum of C10-SPN. (b) The fluorescence emission spectra of C10-SPN. (c) The DLS spectrum of C10-SPN (illustration is the image obtained using a transmission electron microscope). (d) Specificity of C10-SPN against $O_2^{\bullet-}$.

Quantitative analysis using the IVIS imaging system revealed a significant increase in luminescence intensity upon $O_2^{\bullet-}$ exposure, compared to the untreated control (Fig. 3a). These results confirm the strong and specific chemiluminescence response of C10-SPN to $O_2^{\bullet-}$.

To further evaluate the luminescence performance of C10-SPN, its CL half-life was measured. As shown in Fig. 3b, the C10-SPN system exhibited a prolonged half-life of up to 7 min, indicating excellent signal persistence. This extended emission duration provides a sufficient time window for real-time *in vivo* imaging, highlighting its potential use as a chemiluminescent probe for $O_2^{\bullet-}$ detection.

The cytotoxicity of C10-SPN nanoparticles toward 4T1 cells was evaluated using the CCK-8 assay. As shown in Fig. 3c, cells were incubated with increasing concentrations of C10-SPN (0, 3.75, 7.5, 15, 30, 60, 120, 240, 480, and 960 μg mL^{-1}) for 24 h. Even at the highest concentration of 960 μg mL^{-1}, the cell viability remained largely unaffected. These results indicate that C10-SPN exhibits low cytotoxicity and excellent biocompatibility, supporting its suitability for safe *in vivo* applications. Building on the excellent performance of the C10-SPN nanoprobe observed *in vitro*, we conducted *in vivo* imaging experiments to assess its ability to detect $O_2^{\bullet-}$ in a mouse model of peritonitis. Four mice were prepared for imaging experiments:

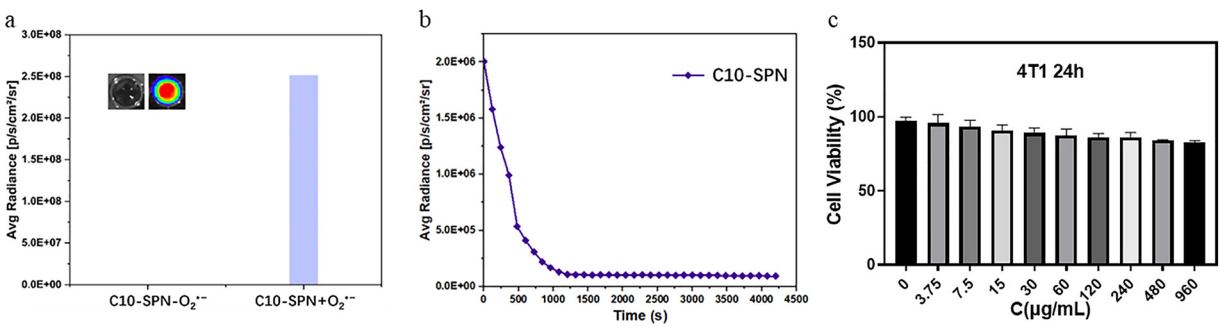

Fig. 3 Chemiluminescence properties of C10-SPN. (a) Relative chemiluminescence intensity. (b) Half-life time of C10-SPN. (c) Cytotoxicity of the prepared C10-SPN probe.

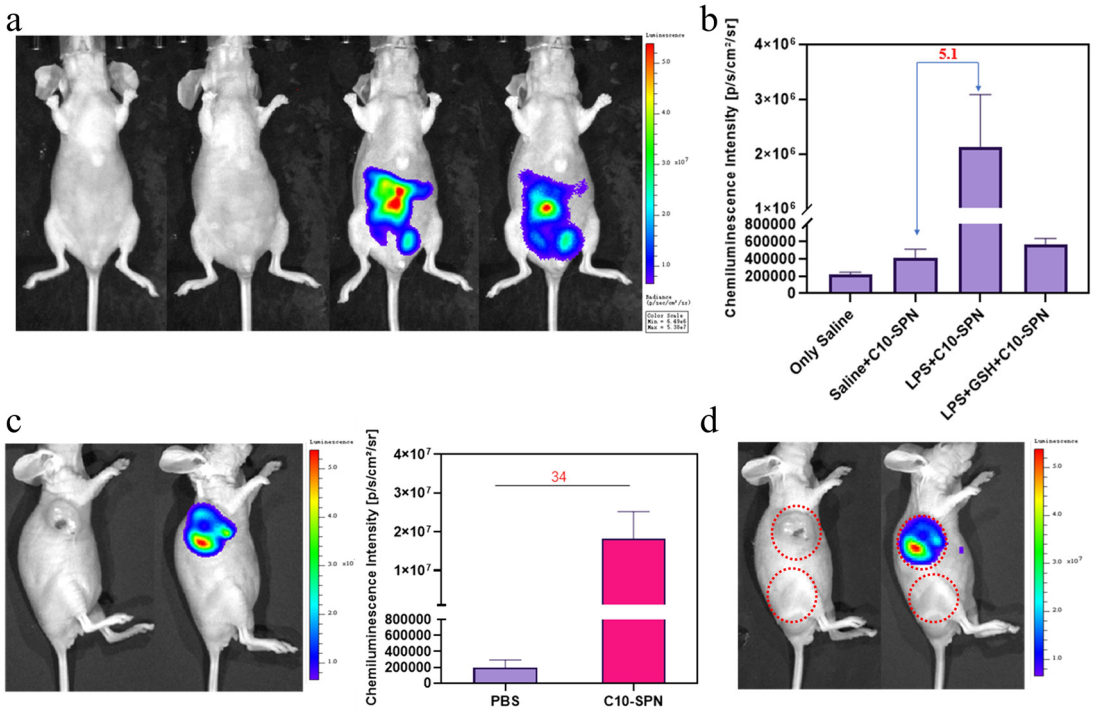

Fig. 4 *In vivo* imaging of inflammation and tumors. (a) Imaging of LPS-induced peritonitis. (b) Statistical comparison of the imaging ability of C10-SPN in different mice. (c) Imaging of the 4T1 cell xenografted tumor and statistical comparison of the imaging ability of C10-SPN and PBS. (d) Comparison of the imaging ability of C10-SPN in tumor and healthy areas.

the first one received saline injection as a background control, the second one received saline and C10-SPN, the third one was injected with lipopolysaccharide (LPS for inducing inflammation)[13,14] and C10-SPN, and the fourth one was injected with LPS, glutathione (GSH), and C10-SPN, with GSH being used to scavenge reactive oxygen species (ROS). Luminescence signals in the abdominal region were then detected using the IVIS imaging system. As shown in Fig. 4a, a strong luminescence signal was observed in the abdominal region in the third mouse, indicating successful induction of inflammation and elevated $O_2^{\bullet-}$ levels. In contrast, no noticeable signal was detected in the second mouse, confirming the specificity of C10-SPN for $O_2^{\bullet-}$. Notably, although inflammation was also induced in the fourth mouse, the presence of GSH reduced the ROS levels, resulting in markedly weaker luminescence compared to that of the third one (Fig. 4b). These findings demonstrate that the C10-SPN nanoprobe enables specific *in vivo* imaging of $O_2^{\bullet-}$ and holds great potential for the visual diagnosis of inflammation-related pathologies.

To further evaluate the ability of the C10-SPN nanoprobe to detect tumors *in vivo*, we established two 4T1 breast cancer xenograft mouse models. In the first mouse, PBS was injected into the tumor site as a control, while in the second mouse, C10-SPN was administered at the tumor site. Subsequently, full-spectrum chemiluminescence signals from both tumor regions were detected using the IVIS imaging system. As shown in Fig. 4c, the tumor site of the C10-SPN-injected mouse exhibited strong chemiluminescence, indicating effective detection of $O_2^{\bullet-}$ within the tumor. Quantitative analysis revealed that the CL intensity in the C10-SPN group was approximately 34 times higher than that of the PBS control, demonstrating a substantial enhancement in signal contrast and detection sensitivity. These findings highlight the strong potential of C10-SPN for tumor-targeted $O_2^{\bullet-}$ imaging *in vivo*.

Notably, to investigate whether the C10-SPN nanoprobe can distinguish tumor tissue from normal tissue *in vivo*, we simultaneously injected PBS or C10-SPN into both the normal and tumor regions of the same mouse. As shown in Fig. 4d, mice injected with PBS exhibited negligible luminescence, whereas those injected with C10-SPN showed significantly stronger chemiluminescence signals at the tumor site compared to normal tissue. These results demonstrate that the C10-SPN nanoprobe can effectively differentiate between healthy and tumor tissues, highlighting its potential for tumor-specific imaging.

In summary, we have developed a novel chemiluminescent nanoprobe, C10-SPN, based on a bicyclic dioxetane scaffold and chemiluminescence resonance energy transfer (CRET) for the selective and sensitive detection of superoxide anion radicals ($O_2^{\bullet-}$) *in vitro* and *in vivo*. The nanoprobe exhibits excellent physicochemical properties, including efficient energy transfer, red-shifted emission at 680 nm, prolonged luminescence duration, and high stability in aqueous environments. C10-SPN shows remarkable specificity toward $O_2^{\bullet-}$ over other reactive oxygen species and ions, along with low cytotoxicity and favorable biocompatibility. *In vivo* studies in mouse models of peritonitis and breast cancer confirmed the nanoprobe's ability

to visualize $O_2^{\bullet-}$ with high spatial resolution and signal contrast, enabling precise differentiation between inflamed or tumor tissues and normal tissues. Importantly, C10-SPN demonstrated excellent performance in distinguishing tumor regions from healthy tissues within the same animal, further validating its potential for accurate tumor-targeted imaging.

Conflicts of interest

The authors declare no competing financial interest.

Data availability

The data supporting this article have been included as part of the supplementary information (SI). Supplementary information: the general procedures of probe 5 synthesis; the characterization of CL probe 5; ^{1}H NMR and ^{13}C NMR spectra of CL probe 5 and *in vitro* and *in vivo* imaging. See DOI: **https://doi.org/10.1039/d5qm00620a**.

Acknowledgements

This work was supported by the National Key Research and Development Program of China (No. 2023YFC3402900), Zhejiang Provincial Science and Technology Plan Project (No. 2024SDYXS0002), and The Independent Deployment Project of the Hangzhou Institute of Medicine, CAS (No. 2024ZZBS03).

References

1 (*a*) S. K. Bardaweel, M. Gul, M. Alzweiri, A. Ishaqat, H. A. ALSalamat and R. M. Bashatwah, Reactive Oxygen Species: the Dual Role in Physiological and Pathological Conditions of the Human Body, *Eurasian J Med.*, 2018, **50**, 193–201; (*b*) G. Maulucci, G. Bačić, L. Bridal, H. H. Schmidt, B. Tavitian, T. Viel, H. Utsumi, A. S. Yalçın and M. De Spirito, Imaging Reactive Oxygen Species-Induced Modifications in Living Systems, *Antioxid. Redox. Signal.*, 2016, **24**, 939–958; (*c*) Y. Cao, J. Gu, Z. Chen, J. Gao, J. Yang, W. Wu, M. Fang, Q. Li, B. Liu and Z. Li, HClO-Activated Near-Infrared Chemiluminescent Probes with a Malononitrile Group for In-Vivo Imaging, *Adv. Mater.*, 2025, **37**, e2408941.

2 (*a*) A. B. Jena, R. R. Samal, N. K. Bhol and A. K. Duttaroy, Cellular Red-Ox System in Health and Disease: The Latest Update, *Biomed. Pharmacother.*, 2023, **162**, 114606; (*b*) A. V. Kozlov, S. Javadov and N. Sommer, Cellular ROS and Antioxidants: Physiological and Pathological Role, *Antioxidants*, 2024, **13**, 602.

3 (*a*) J. Checa and J. M. Aran, Reactive Oxygen Species: Drivers of Physiological and Pathological Processes, *J. Inflammation Res.*, 2020, **13**, 1057–1073; (*b*) M. Valko, D. Leibfritz, J. Moncol, M. T. Cronin, M. Mazur and J. Telser, Free Radicals and Antioxidants in Normal Physiological Functions and Human Disease, *Int. J. Biochem. Cell Biol.*, 2007, **39**, 44–84; (*c*) K. Jomova, R. Raptova, S. Y. Alomar, S. H. Alwasel, E. Nepovimova, K. Kuca and M. Valko, Reactive Oxygen Species, Toxicity, Oxidative Stress, and Antioxidants: Chronic Diseases and Aging, *Arch. Toxicol.*, 2023, **97**, 2499–2574.

4 W. Zhang, P. Li, F. Yang, X. Hu, C. Sun, W. Zhang, D. Chen and B. Tang, Dynamic and Reversible Fluorescence Imaging of Superoxide Anion Fluctuations in Live Cells and In Vivo, *J. Am. Chem. Soc.*, 2013, **135**, 14956–14959.

5 H. Xiao, W. Zhang, P. Li, W. Zhang, X. Wang and B. Tang, Versatile Fluorescent Probes for Imaging the Superoxide Anion in Living Cells and In Vivo, *Angew. Chem., Int. Ed.*, 2020, **59**, 4216–4230.

6 Y. Zhou, X. Kuang, X. Yang, J. Li, X. Wei, W. J. Jang, S. S. Zhang, M. Yan and J. Yoon, Recent progress in small-molecule fluorescent probes for the detection of superoxide anion, nitric oxide, and peroxynitrite anion in biological systems, *Chem. Sci.*, 2024, **15**, 19669–19697.

7 (*a*) C. Huang, W. Zhou, R. Wu, W. Guan and N. Ye, Recent Advances in Nanomaterial-Based Chemiluminescence Probes for Biosensing and Imaging of Reactive Oxygen Species, *Nanomaterials*, 2023, **13**, 1726; (*b*) J. S. Kim, K. Jeong, J. M. Murphy, Y. A. R. Rodriguez and S. S. Lim, A Quantitative Method to Measure Low Levels of ROS in Nonphagocytic Cells by Using a Chemiluminescent Imaging System, *Oxid. Med. Cell. Longevity*, 2019, **2019**, 1754593.

8 (*a*) Y. Cao, J. Yang, B. Liu and Z. Li, Recent Progress in Small Molecule-Based Chemiluminescent Probes for Reactive Oxygen and Nitrogen Species, *Chem. Biomed. Imaging*, 2025, DOI: **10.1021/cbmi.5c00043**; (*b*) T. Meng, X. Zhang, W. Tang, C. Liu and X. Duan, A Small Molecule Chemiluminophore with near 600 nm Emission for In Vivo Imaging of Myeloperoxidase and Inflammatory Diseases, *Chem. Biomed. Imaging*, 2024, **2**, 205–212; (*c*) Q. Shang, S. H. Li, Y. T. He, Y. Zhang, T. Fu, S. S. Han, W. Huang, X.-Q. Wang and J. H. Xu, High Contrast Bioimaging of Tumor and Inflammation with a Bicyclic Dioxetane Chemiluminescent Probe, *Anal. Chem.*, 2024, **96**, 2286–2291; (*d*) M. Shi, Y. Zhang, J. X. Chen, Y. Wu, Z. Wang, P. F. Shi, X. Jin and X.-Q. Wang, A Bicyclic Dioxetane Chemiluminescence Nanoprobe for Peroxynitrite Imaging in Vivo, *Anal. Chem.*, 2024, **96**, 19109–19116.

9 S. H. Li, G. R. Zhang, Y. T. He, L. Yang, H. L. Li, C. Y. Long, Y. Cui and X.-Q. Wang, Emission Wavelength-Tunable Bicyclic Dioxetane Chemiluminescent Probes for Precise In Vitro and In Vivo Imaging, *Anal. Chem.*, 2023, **95**, 13191–13200.

10 (*a*) J. Huang, J. Huang, P. Cheng, Y. Jiang and K. Pu, Near-Infrared Chemiluminescent Reporters for In Vivo Imaging of Reactive Oxygen and Nitrogen Species in Kidneys, *Adv. Funct. Mater.*, 2020, **30**, 2003628; (*b*) Q. Miao, C. Xie, X. Zhen, Y. Lyu, H. Duan, X. Liu, J. V. Jokerst and K. Pu, Molecular Afterglow Imaging with Bright, Biodegradable Polymer Nanoparticles, *Nat. Biotechnol.*, 2017, **35**, 1102–1110.

11 X. Wang, Q. Ding, R. R. Groleau, L. Wu, Y. Mao, F. Che, O. Kotova, E. M. Scanlan, S. E. Lewis and P. Li, Fluorescent

probes for disease diagnosis, *Chem. Rev.*, 2024, **124**, 7106–7164.

12 J. J. Hu, N. K. Wong, S. Ye, X. Chen, M. Y. Lu, A. Q. Zhao, Y. Guo, A. C. H. Ma, A. Y. H. Leung, J. Shen and D. Yang, Fluorescent probe HKSOX-1 for imaging and detection of endogenous superoxide in live cells and in vivo, *J. Am. Chem. Soc.*, 2015, **137**, 6837–6843.

13 K. Bedard and K. H. Krause, The NOX Family of ROS-Generating NADPH Oxidases: Physiology and Pathophysiology, *Physiol. Rev.*, 2007, **87**, 245–313.

14 M. Canton, R. Sánchez-Rodríguez, I. Spera, F. C. Venegas, M. Favia, A. Viola and A. Castegna, Reactive Oxygen Species in Macrophages: Sources and Targets, *Front. Immunol.*, 2021, **12**, 734229.